Research Article | Vol. 26, No. 5 | 5 Mar 2018 | OPTICS EXPRESS 5800

Optics EXPRESS

Demonstration of versatile whispering-gallery micro-lasers for remote refractive index sensing

LEI WAN,[1,2,11] HENGKY CHANDRAHALIM,[3,4,11] JIAN ZHOU,[2,5,11] ZHAOHUI LI,[1] CONG CHEN,[2,6] SANGHA CHO,[7] HUI ZHANG,[8] TING MEI,[9] HUIPING TIAN,[5] YUJI OKI,[6] NAOYA NISHIMURA,[10] XUDONG FAN,[4,12] AND L. JAY GUO[2,13]

[1]*State Key Laboratory of Optoelectronic Materials and Technologies and School of Electronics and Information Technology, Sun Yat-Sen University, Guangzhou 511400, China*
[2]*Department of Electrical Engineering and Computer Science, University of Michigan, Ann Arbor, Michigan 48109, USA*
[3]*Department of Electrical and Computer Engineering, The Air Force Institute of Technology, Wright-Patterson AFB, Ohio 45433, USA*
[4]*Department of Biomedical Engineering, University of Michigan, Ann Arbor, Michigan 48109, USA*
[5]*School of Information and Communication Engineering, Beijing University of Posts and Telecommunications, Beijing 100876, China*
[6]*Graduate School and Faculty of Information Science and Electrical Engineering, Kyushu University, Fukuoka 819 0395, Japan*
[7]*Department of Engineering Physics, University of Michigan, Ann Arbor, Michigan 48109, USA*
[8]*School of Physics and Optoelectronic Engineering, Guangdong University of Technology, Guangzhou 510006, China*
[9]*School of Science, Northwestern Polytechnical University, Xi'an 710072, China*
[10]*Nissan Chemical Industries, Ltd, 488-6, Suzumi-cho, Funabashi 274-0052, Japan*
[11]*These authors contributed equally to this work.*
[12]*xsfan@umich.edu*
[13]*guo@umich.edu*

Abstract: We developed chip-scale remote refractive index sensors based on Rhodamine 6G (R6G)-doped polymer micro-ring lasers. The chemical, temperature, and mechanical sturdiness of the fused-silica host guaranteed a flexible deployment of dye-doped polymers for refractive index sensing. The introduction of the dye as gain medium demonstrated the feasibility of remote sensing based on the free-space optics measurement setup. Compared to the R6G-doped TZ-001, the lasing behavior of R6G-doped SU-8 polymer micro-ring laser under an aqueous environment had a narrower spectrum linewidth, producing the minimum detectable refractive index change of 4×10^{-4} RIU. The maximum bulk refractive index sensitivity (BRIS) of 75 nm/RIU was obtained for SU-8 laser-based refractive index sensors. The economical, rapid, and simple realization of polymeric micro-scale whispering-gallery-mode (WGM) laser-based refractive index sensors will further expand pathways of static and dynamic remote environmental, chemical, biological, and bio-chemical sensing.

OCIS codes: (140.3460) Lasers; (140.4780) Optical resonators; (130.5460) Polymer waveguides; (130.6010) Sensors.

References and links

1. A. L. Washburn, L. C. Gunn, and R. C. Bailey, "Label-free quantitation of a cancer biomarker in complex media using silicon photonic microring resonators," Anal. Chem. **81**(22), 9499–9506 (2009).
2. G. Bahl, K. H. Kim, W. Lee, J. Liu, X. Fan, and T. Carmon, "Brillouin cavity optomechanics with microfluidic devices," Nat. Commun. **4**(3), 1994 (2013).
3. A. M. Armani and K. J. Vahala, "Heavy water detection using ultra-high-Q microcavities," Opt. Lett. **31**(12), 1896–1898 (2006).

#318879 https://doi.org/10.1364/OE.26.005800
Journal © 2018 Received 3 Jan 2018; revised 19 Feb 2018; accepted 20 Feb 2018; published 26 Feb 2018

Optics EXPRESS

4. V. R. Dantham, S. Holler, V. Kolchenko, Z. Wan, and S. Arnold, "Taking whispering gallery-mode single virus detection and sizing to the limit," Appl. Phys. Lett. **101**(4), 043704 (2012).
5. F. Vollmer and S. Arnold, "Whispering-gallery-mode biosensing: label-free detection down to single molecules," Nat. Methods **5**(7), 591–596 (2008).
6. L. Shao, X. F. Jiang, X. C. Yu, B. B. Li, W. R. Clements, F. Vollmer, W. Wang, Y. F. Xiao, and Q. Gong, "Detection of single nanoparticles and lentiviruses using microcavity resonance broadening," Adv. Mater. **25**(39), 5616–5620 (2013).
7. S. H. Huang, S. Sheth, E. Jain, X. Jiang, S. P. Zustiak, and L. Yang, "Whispering gallery mode resonator sensor for in situ measurements of hydrogel gelation," Opt. Express **26**(1), 51–62 (2018).
8. L. He, S. K. Ozdemir, J. Zhu, and L. Yang, "Ultrasensitive detection of mode splitting in active optical microcavities," Phys. Rev. A **82**(5), 11992–12003 (2010).
9. R. K. Chang and A. J. Campillo, *Optical Processes in Microcavities* (World Scientific, 1996).
10. D. K. Armani, T. J. Kippenberg, S. M. Spillane, and K. J. Vahala, "Ultra-high-Q toroid microcavity on a chip," Nature **421**(6926), 925–928 (2003).
11. X. Jiang, L. Shao, S. X. Zhang, X. Yi, J. Wiersig, L. Wang, Q. Gong, M. Lončar, L. Yang, and Y. F. Xiao, "Chaos-assisted broadband momentum transformation in optical microresonators," Science **358**(6361), 344–347 (2017).
12. Y. C. Lin, M. H. Mao, C. J. Wu, and H. H. Lin, "InAsSb/InAsPSb multiple quantum well disk cavities with pedestal structures on a GaSb substrate for mid-infrared whispering-gallery-mode emission beyond 4 μm," Opt. Lett. **40**(9), 1904–1907 (2015).
13. V. S. Ilchenko, X. S. Yao, and L. Maleki, "Pigtailing the high-Q microsphere cavity: a simple fiber coupler for optical whispering-gallery modes," Opt. Lett. **24**(11), 723–725 (1999).
14. J. P. Laine, B. E. Little, D. R. Lim, H. C. Tapalian, L. C. Kimerling, and H. A. Haus, "Microsphere resonator mode characterization by pedestal anti-resonant reflecting waveguide coupler," IEEE Photonics Technol. Lett. **12**(8), 1004–1006 (2000).
15. Y. L. Pan and R. K. Chang, "Highly efficient prism coupling to whispering gallery modes of a square μ-cavity," Appl. Phys. Lett. **82**(4), 487–489 (2003).
16. J. C. Knight, G. Cheung, F. Jacques, and T. A. Birks, "Phase-matched excitation of whispering-gallery-mode resonances by a fiber taper," Opt. Lett. **22**(15), 1129–1131 (1997).
17. T. Kato, W. Yoshiki, R. Suzuki, and T. Tanabe, "Polygonal silica toroidal microcavity for controlled optical coupling," Appl. Phys. Lett. **101**(12), 121101 (2012).
18. V. B. Braginsky, M. L. Gorodetsky, and V. S. Ilchenko, "Quality-factor and nonlinear properties of optical whispering-gallery modes," Phys. Lett. A **137**(7), 393–397 (1989).
19. S. M. Spillane, T. J. Kippenberg, O. J. Painter, and K. J. Vahala, "Ideality in a fiber-taper-coupled microresonator system for application to cavity quantum electrodynamics," Phys. Rev. Lett. **91**(4), 043902 (2003).
20. Z. Guo, H. Quan, and S. Pau, "Near-field gap effects on small microcavity whispering-gallery mode resonators," J. Phys. D Appl. Phys. **39**(24), 5133–5136 (2006).
21. C. Zhao, Q. Yuan, L. Fang, X. Gan, and J. Zhao, "High-performance humidity sensor based on a polyvinyl alcohol-coated photonic crystal cavity," Opt. Lett. **41**(23), 5515–5518 (2016).
22. K. Kosma, G. Zito, K. Schuster, and S. Pissadakis, "Whispering gallery mode microsphere resonator integrated inside a microstructured optical fiber," Opt. Lett. **38**(8), 1301–1303 (2013).
23. J. Yang and L. J. Guo, "Optical sensors based on active-microcavities," IEEE J. Sel. Top. Quantum Electron. **12**(1), 143–147 (2006).
24. Z. P. Liu, X. F. Jiang, Y. Li, Y. F. Xiao, L. Wang, J. L. Ren, S. J. Zhang, H. Yang, and Q. H. Gong, "High-Q asymmetric polymer microcavities directly fabricated by two-photon polymerization," Appl. Phys. Lett. **102**(22), 221108 (2013).
25. A. Francois and M. Himmelhaus, "Whispering gallery mode biosensor operated in the stimulated emission regime," Appl. Phys. Lett. **94**(3), 031101 (2009).
26. S. Pang, R. E. Beckham, and K. E. Meissner, "Quantum dot-embedded microspheres for remote refractive index sensing," Appl. Phys. Lett. **92**(22), 221108 (2008).
27. A. François, N. Riesen, K. Gardner, T. M. Monro, and A. Meldrum, "Lasing of whispering gallery modes in optofluidic microcapillaries," Opt. Express **24**(12), 12466–12477 (2016).
28. S. Krämmer, S. Rastjoo, T. Siegle, S. F. Wondimu, C. Klusmann, C. Koos, and H. Kalt, "Size-optimized polymeric whispering gallery mode lasers with enhanced sensing performance," Opt. Express **25**(7), 7884–7894 (2017).
29. H. Chandrahalim and X. Fan, "Reconfigurable solid-state dye-doped polymer ring resonator lasers," Sci. Rep. **5**(1), 18310 (2015).
30. X. F. Jiang, C. L. Zou, L. Wang, Q. H. Gong, and Y. F. Xiao, "Whispering-gallery microcavities with unidirectional laser emission," Laser Photonics Rev. **10**(1), 40–61 (2016).
31. X. Xu, X. Jiang, G. Zhao, and L. Yang, "Phone-sized whispering-gallery microresonator sensing system," Opt. Express **24**(23), 25905–25910 (2016).
32. L. Wan, H. Chandrahalim, C. Chen, Q. S. Chen, T. Mei, Y. Oki, N. Nishimura, L. J. Guo, and X. D. Fan, "On-chip, high-sensitivity temperature sensors based on dye-doped solid-state polymer microring lasers," Appl. Phys. Lett. **111**(6), 061109 (2017).

Optics EXPRESS

33. H. Chandrahalim, Q. Chen, A. A. Said, M. Dugan, and X. Fan, "Monolithic optofluidic ring resonator lasers created by femtosecond laser nanofabrication," Lab Chip **15**(10), 2335–2340 (2015).
34. J. Li, Y. Lin, J. Lu, C. Xu, Y. Wang, Z. Shi, and J. Dai, "Single mode ZnO whispering-gallery submicron cavity and graphene improved lasing performance," ACS Nano **9**(7), 6794–6800 (2015).
35. H. Chandrahalim, S. C. Rand, and X. Fan, "Evanescent coupling between refillable ring resonators and laser-inscribed optical waveguides," Appl. Opt. **56**(16), 4750–4756 (2017).
36. J. W. Silverstone, S. McFarlane, C. P. K. Manchee, and A. Meldrum, "Ultimate resolution for refractometric sensing with whispering gallery mode microcavities," Opt. Express **20**(8), 8284–8295 (2012).
37. H. Yan, L. Huang, X. Xu, S. Chakravarty, N. Tang, H. Tian, and R. T. Chen, "Unique surface sensing property and enhanced sensitivity in microring resonator biosensors based on subwavelength grating waveguides," Opt. Express **24**(26), 29724–29733 (2016).
38. C. Chen, L. Wan, H. Chandrahalim, J. Zhou, H. Zhang, S. Cho, T. Mei, H. Yoshioka, H. Tian, N. Nishimura, X. Fan, L. J. Guo, and Y. Oki, "The effects of edge inclination angles on whispering-gallery modes in printable wedge microdisk lasers," Opt. Express **26**(1), 233–241 (2018).
39. J. B. Abshire, A. Ramanathan, H. Riris, J. Mao, G. R. Allan, W. E. Hasselbrack, C. J. Weaver, and E. V. Browell, "Airborne measurements of CO_2 column concentration and range using a pulsed direct-detection IPDA lidar," Remote Sens. **6**(1), 443–469 (2014).

1. Introduction

We rely on the use of various sensors in our modern lives. This is more true than ever in the eminent internet-of-things (IoT) era, where massive deployment of sensors is anticipated. There are scenarios and environments where direct human participation is not possible for making measurements, and thus remote sensing is highly desirable.

High-sensitivity and label-free optical sensors are crucial for a wide range of applications, such as clinical diagnostics [1], environmental monitoring [2, 3], and public health [4]. With high quality factors (Q-factors) and strong light-matter interactions, WGM cavities have great potential to provide us with a label-free [5–7], ultra-sensitive detection [8]. A key feature of WGMs is the evanescent field that interacts with the surrounding medium, causing the spectral position to change with external refractive index or adsorption of molecular layers onto the resonator surfaces. In addition, compared to the straight waveguides with the same percentage of evanescent light, WGM resonators could readily allow for miniaturization of sensors [9].

Silica based WGM resonators with diverse geometries, such as sphere [4], toroid [10, 11], ring [1], and disk [12] have been prominently investigated. They are also the possible candidates for the remote sensing of the environment by measuring the index change caused by various factors.

The vast majority of the resonators studied are passive, requiring a tapered optical fiber [13], an optical ridge waveguide [14] or a prism [15] to couple light to the cavity modes. These resonators require a precise coupling distance and element sizes to fulfill the phase matching conditions [16–18]. Although remarkable coupling efficiencies and high Q-factors of the passive WGM resonators can be obtained [19], the requirements for external evanescent field coupling configurations may hinder some real-life applications outside the laboratory. Furthermore, due to the influence of spectral position changes by external couplers, the actual signal would be unstable [20]. Free-space measurement setups may make such passive-cavity based optical sensing feasible [21, 22]; however, lower signal intensity and polarization dependent directional scattering limits its applications in diverse geometrical resonators.

On the other hand, active cavities that contain an optical gain medium can in principle provide higher sensitivity [23, 24], and are particularly suited to remote pumping and collection of the amplified spontaneous emission or lasing signals via free-space optics. In an active optical resonator, the loss (i.e. absorption loss, radiation loss, and scattering loss) can be compensated by the gain medium, which will increase Q-factor of the resonance and narrow the line widths, hence increasing the sensitivity of detection limit (DL). Recently, active WGM resonator-based sensors have achieved good progress in terms of sensitivity or DL enhancement based on a spectral shift regime. The active micro-spheres operated in the

Optics EXPRESS

stimulated emission state have demonstrated eight-fold signal-to-noise ratio (SNR) improvements and a three-fold Q-factor enhancement which helps the real-time detection of absorption kinetics of bovine serum albumin in phosphate buffered saline [25]. Similarly, quantum dots (QDs)-embedded with polystyrene (PS) micro-spheres have been used for refractive index sensing with the experimentally enhanced sensitivity of approximately 160 nm/RIU (refractive index unit) [26]. Fluorescent dye-doped (Nile Red) polymer coatings with different thicknesses embedded inside silica capillaries have been applied for optofluidic refractive index sensors with improved DL of 1.2×10^{-3} and a sensitivity of 3 nm/RIU [27]. Size-optimized polymeric micro-disk cavities with the optical gain material Pyrromethene 597 have been developed to boost the BRIS to 150 nm/RIU with a Q-factor of 10^5 [28]. In addition, compared to the inorganic semiconductors, gain medium doped polymers are more easily fabricated into high-Q WGM resonators due to their outstanding flexibility and simple preparation methods.

In this paper, in order to realize a simple, robust, and versatile platform for remote refractive index sensing, organic dye R6G-doped polymer SU-8 and TZ-001 micro-ring lasers were fabricated in sequence on the fused-silica wafer with patterned microring template. The characterizations of the polymer laser-based refractive index sensors were performed based on a free-space optics measurement setup. The optical parameters of the micro-scale lasers were estimated to verify the feasibility of refractive index sensing in aqueous environments. After that, the lemon juice and water were repeatedly replaced to observe the lasing peak shift induced by an environmental index change. As a result, the sensitivities and detection limits of both polymer refractive index sensors were reported, respectively.

2. Experiment

2.1 Fabrication of micro-ring laser based refractive index sensor

The solid-state polymer micro-ring laser-based refractive index sensor used in this work consisted of a fused-silica micro-ring with a channel profile as a cladding layer and a cured R6G-doped polymer gain material deposited on it as a core layer. For the R6G-doped SU-8 polymer micro-ring resonator, R6G was first dissolved in ethanol with a dye concentration of 10 mM and subsequently mixed with SU-8 at a volume ratio of 10% (ethanol + dye) to 90% (SU-8) in an ultrasonic bath for 5 minutes. Next, the R6G-doped SU-8 with a dye concentration of 1 mM was dripped and spin-coated on the patterned fused-silica chips and baked at 95 °C for 15 minutes to evaporate the solvent and cure the polymer. Similarly, for the R6G-doped TZ-001 polymer micro-ring resonator, TZ-001 powder was first dissolved in cyclohexanone with a concentration of 10% (by weight) in an ultrasonic bath for 6 hours to form solution A. Subsequently, R6G was mixed with solution A in the ultrasound bath for 4 hours to form solution B with a dye concentration of 5 mM. Next, solution A was mixed with solution B at a volume ratio of 4:1 in the ultrasonic bath for 5 minutes. Finally, the resultant dye-doped polymer solution was spin-coated on the patterned fused-silica sample and cured at room temperature overnight. After the solvent was evaporated, the polymer coating around the sidewalls of silica trench channel formed two micro-ring resonator lasers along inner and outer circumferences of the ring. Figure 1 illustrates the top and cross-sectional views of the active WGMs resonator-based refractive index sensor. Figure 2(a) depicts the scanning electron microscope (SEM) image of an etched fused-silica micro-ring resonator host prior to polymer deposition. The fabrication methods of the solid-state polymer core layer are displayed in Figs. 2(b) to 2(d). The detailed fabrication processes were presented in our previous work [29].

Optics EXPRESS

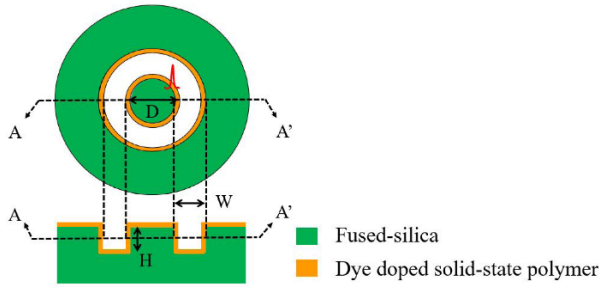

Fig. 1. Top view and cross-sectional view along the AA' plane of a dye-doped solid-state polymer micro-ring laser.

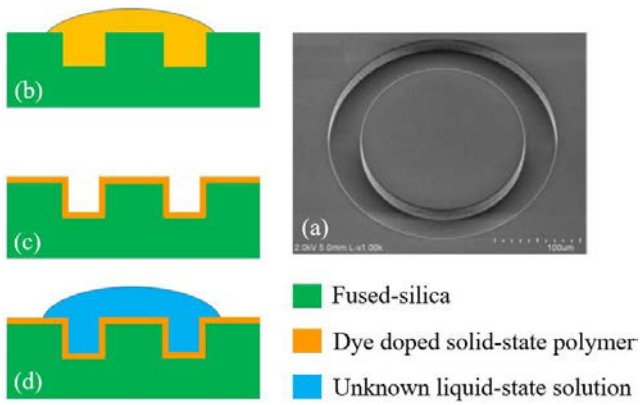

Fig. 2. (a) SEM image of an etched fused-silica micro-ring resonator host with a channel profile. The width (W) and height (H) of this ring resonator host were 40 μm and 30 μm, respectively. The diameter (D) of the inner fused-silica microdisc was 220 μm. (b)-(d) Cross-sectional views corresponding to a dye-doped liquid-state polymer (b) dripped, (c) spin-coated, and (d) cured on the patterned wafer.

2.2 Measurement setup

For the passive micro-ring resonator with the similar trench structure, the readout of mode is difficult to readily realize based on common fiber coupling methods, especially for the inner micro-ring, which limits its potential application as refractive index sensor. On the contrary, for the active micro-ring laser, the lasing signal from trench structure could be readily collected using a free-space optics measurement setup. Meanwhile, the trench channel profile can function as a microfluidic chamber for various solutions. These advantages increase the sensing performance of micro-ring lasers as refractive index sensors. A free-space optics measurement system is provided in Fig. 3. Optical experiments were conducted using a pulsed nanosecond laser with an optical parameter oscillator (OPO) (repetition rate: 20 Hz, pulse width: 5 ns), a spectrometer (Horiba 550) with a 2400 l/mm grating, and an objective lens with a 20 mm working distance. When the polymer WGMs micro-ring laser was completely covered by the focused pump light, the scattered lasing signals [30] from the polymer laser passed through a beam splitter and were focused into a spectrometer inlet using a lens. Here, the focused spot area of the pump light on the sample was approximately 0.07 mm^2 using an objective lens. A charge coupled device (CCD) camera was used to monitor the position of the micro-ring resonator laser relative to the center of the transmitted pump light spot. To perform experiments in aqueous environments, a plastic petri dish allowing for resonator samples immersed in liquids was placed to investigate the refractive index sensing. In order to satisfy the miniature requirement of the IoT system in the future, the bulky measurement components could be reduced to much smaller format, like those integrated into

Optics EXPRESS

phone-sized embedded systems described in Ref [31], which could make the whole free-space optics measurement setup into a portable active WGM testing system.

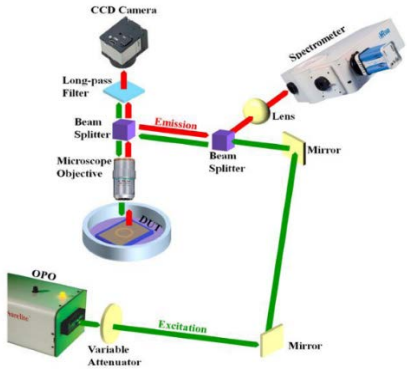

Fig. 3. Illustration of the measurement setup for the dye-doped solid-state polymer micro-ring resonator laser-based refractive index sensor.

3. Characterization and discussion

As shown in Fig. 4(a), the lasing spectral characteristics of a R6G-doped SU-8 polymer micro-ring laser was demonstrated in an aqueous environment. The full width at half maximum (FWHM) of the lasing peak at approximately 593.91 nm was measured to be 0.034 nm, which was similar to the value of FWHM measured in air [32]. We have also measured laser emissions from various fluidic gain media that fill the entire ring resonator template [33] and recorded a comparable laser line width. Here the characterization of optofluidic lasers would further accelerate the development of WGM micro-scale lasers. Using the equation for the Q-factor of a passive resonator ($Q = \lambda/\Delta\lambda$) [34], the corresponding Q-factor for this R6G-doped polymer micro-ring laser in water was estimated to be 1.75×10^4. The relatively low Q-factor was mainly due to the scattering losses in the optical ring resonators. We have extensively characterized the performances of similar passive ring resonators of for one month [35]. The free spectrum range (FSR) was measured to be 0.286 nm. The decreased FSR was mainly attributed to the increased effective refractive index of polymer micro-ring resonator under an aqueous environment in comparison with that in air. Given the chemical resistance of SU-8 polymer towards water molecules, the radius of the micro-ring laser was estimated to be approximately 115.4 μm according to our previous work [32], suggesting that the laser emissions originated mainly from the inner circumference of the micro-ring.

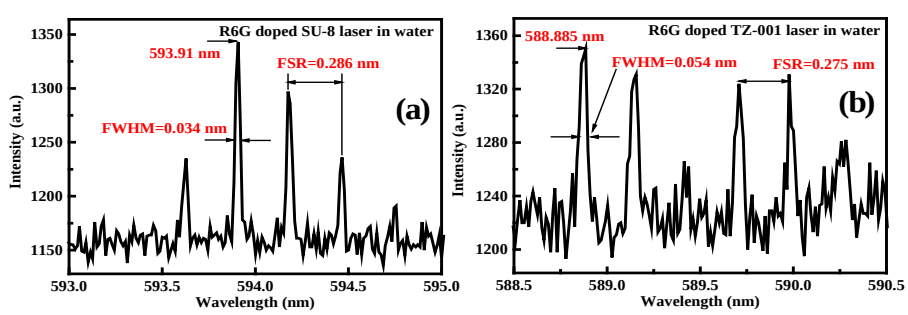

Fig. 4. Comparison of the lasing spectral characteristics between (a) R6G-doped SU-8 polymer micro-ring laser and (b) R6G-doped TZ-001 polymer micro-ring laser in water.

To estimate the lifetime and photostability of SU-8 polymer micro-ring lasers under the aqueous environment, the lasing threshold was characterized and the lasing spectra was compared at different time intervals. Figure 5(a) shows that the lasing threshold was

Optics EXPRESS

measured to be 2.52 μJ/mm^2, which is two times higher than that in air. This was mainly caused by the increased propagation loss in water. The lasing spectra in Fig. 6(a) were measured under the pump energy intensity of 35.2 μJ/mm^2. These spectra were collected with a time interval of 30 s. The relatively immobilized lasing wavelength position demonstrated the good photostability of R6G-doped SU-8 polymer micro-ring laser under an aqueous environment. The zoomed-in lasing peak at 599.8 nm as the spectral marker in Fig. 6(b) exhibited a total spectral shift of less than 0.021 nm even under a high pump energy intensity.

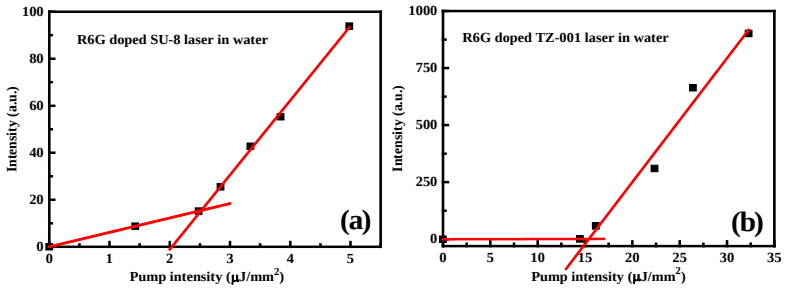

Fig. 5. Comparison of the lasing thresholds between (a) R6G-doped SU-8 polymer micro-ring laser and (b) R6G-doped TZ-001 polymer micro-ring laser in water.

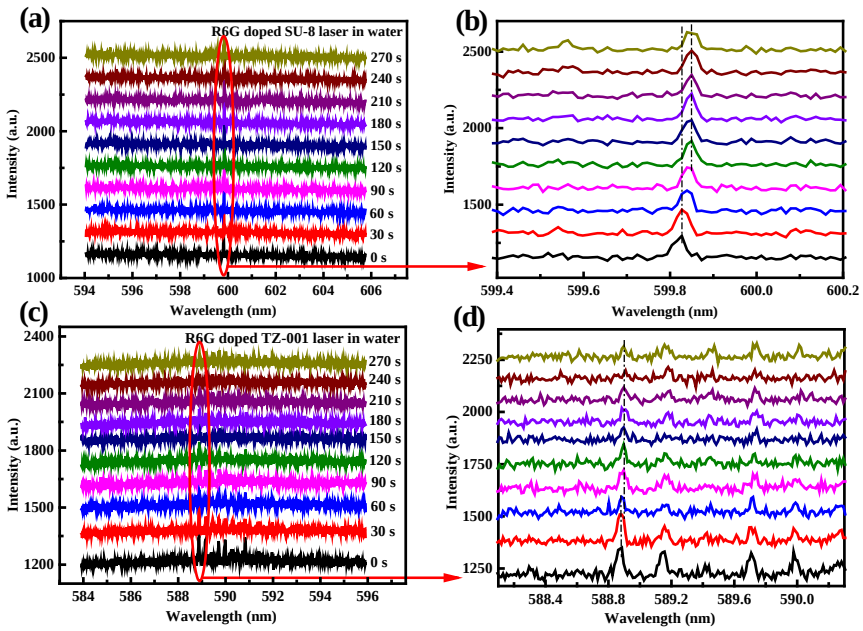

Fig. 6. Lasing spectra collected under different time intervals for the R6G-doped (a) SU-8 polymer micro-ring laser and (c) TZ-001 polymer micro-ring laser in water. Expansion of the lasing spectra at approximately 599.8 nm for (b) SU-8 and at approximately 588.8 nm for (d) TZ-001.

The characterization of the R6G-doped SU-8 polymer micro-ring laser-based refractive index sensing was performed by repeatedly changing the water into lemon juice. The comparable lasing spectrum properties under each environment demonstrated the stability of polymer micro-ring laser-based refractive index sensor. The refractive index of water was estimated to be 1.3324. The index of 1.3488 was measured using Abbe refractometer for the lemon juice. Before we conducted sensing measurement, the refractive index of lemon juice had been calibrated using the Abbe refractometer, which could guarantee the consistency of variety of lemon juice. Figure 7(a) shows that the lasing spectrum had a redshift of 1.229 nm

Optics EXPRESS

when the water was replaced by lemon juice, demonstrating the increased refractive index change. The contribution of the mode radius can be ignored because the change was small in comparison with the radius (110 μm) of the microcavity. The alternate and repeated lasing spectra were recorded as statistical results of the standard deviations of the lasing wavelength shifts, as shown in Fig. 7(b). The insets show the error ranges of lasing wavelength shifts corresponding to both liquid environments. Considering the linear relationship between the bulk refractive index and resonance wavelength shift, which has been demonstrated before [36, 37], by linear fitting the lasing wavelength shifts of both environments, the BRIS was estimated to be 75 nm/RIU. Compared to the BRIS of QDs-embedded PS microsphere-based sensor [26], which is two times higher than that of our device, the refractive index and distribution of organic dye is not enough to move the confinement of the mode energy closer to the surface of a micro-ring resonator. Meanwhile, the thicker SU-8 core layer polymer suppressed the radiation of the mode. In order to further improve the BRIS of laser-based refractive index sensor, the polymer core-layer with low refractive index could be spin-coated to enhance the interaction between the mode and solution needed to measure due to the large energy leakage. The minimum detectable refractive index change (DL) can be estimated to be 4×10^{-4} RIU, which is limited by the wavelength pitch between two adjacent CCD pixels in the system. The realization of the SU-8 polymer micro-ring laser-based refractive index sensor with a micrometer-sized footprint thereby demonstrates its feasibility in remote environmental, chemical, bio-chemical, and biological sensing.

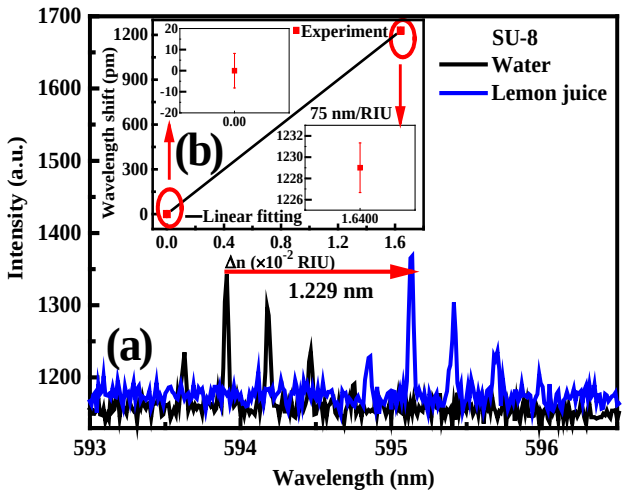

Fig. 7. (a) Lasing spectra of the R6G-doped SU-8 polymer micro-ring laser in water and lemon juice. (b) The inset depicts the lasing peak shifts as a linear function of refractive index change.

In order to demonstrate the versatility and reusability of our micro-ring cavity platform, the R6G-doped SU-8 polymer was removed and R6G-doped TZ-001 polymer was deposited on the same micro-ring host. TZ-001 polymer with refractive index of 1.78 is an exotic polymeric material that has not been extensively investigated. Moreover, TZ-001 micro-lasers with user-defined edge profiles can be mass-produced rapidly and economically by ink-jet printing technique [38], a promising technology to generate a large quantity of micro-laser sensors to the market. The R6G-doped TZ-001 polymer layer with thickness of approximately 0.5 μm thus was spin-coated on the micro-ring resonator host to demonstrate its detection capability for surrounding environmental media.

Figure 4(b) shows the lasing spectral characteristics of R6G-doped TZ-001 polymer laser-based refractive index sensor under an aqueous environment. The FWHM was measured to be 0.054 nm, and the corresponding Q-factor was calculated to be 1.1×10^4. Compared to the case of SU-8, the decreased Q-factor was mainly attributed to the larger scattering loss and

Optics EXPRESS

absorption loss of TZ-001 polymer laser. The FSR was estimated to be 0.275 nm, which is smaller than that of SU-8, due to the higher refractive index of TZ-001 polymer. Considering the immiscibility between the TZ-001 and water, the 0.5 μm-thick TZ-001 polymer layer was preserved in an aqueous environment. The thinner TZ-001 polymer layer in comparison with SU-8 was fabricated due to the brittle property of thick TZ-001 film.

The lasing threshold was measured to be 15.5 μJ/mm^2, which is 1.67 times greater than the measurement in air, and 6.15 times greater than that of SU-8 in water, as shown in Fig. 5(b). The significantly increased lasing threshold was attributed to the absorption loss caused by some cracks in the resonator surface. Similarly, the variations of lasing spectra were collected in a 0 to 270 s time scale to observe photostability of R6G-doped TZ-001 polymer laser-based refractive index sensor in an aqueous environment and the pump energy intensity of 96 μJ/mm^2. The time interval was 30 s, as shown in Fig. 6(c). The high pump intensity was used to increase mode visibility, while mode number tended to increase. The zoomed-in lasing spectra in Fig. 6(d) shows that the SNR of lasing peak gradually decreased with the increase of sampling time, the position change of lasing peak however was maintained within less than 0.011 nm. The quick attenuation rate of R6G-doped TZ-001 polymer laser in water has enforced the use of low-pump intensity to excite the laser.

When the water was replaced by lemon juice, a redshift of 0.047 nm was recorded from TZ-001 laser-based refractive index sensor, as shown in Fig. 8(a). Compared to SU-8, the smaller wavelength shift was mainly caused by larger refractive index and lower Q-factor of cold cavity for the TZ-001. By fitting the wavelength shifts using linear model, the sensitivity of R6G-doped TZ-001 polymer micro-ring laser-based refractive index sensor was calculated to be 3 nm/RIU, as shown in Fig. 8(b). The DL was estimated to be 1×10^{-2} RIU due to the limitation of spectrometer resolution (0.03 nm). Compared to the polymer-embedded micro-capillary laser-based optofluidic refractive index sensor [27], the TZ-001 sensor has comparable sensitivity and DL. The demonstration of both dye-doped SU-8 and TZ-001 has exhibited the flexibility, robustness, and ease of use of our sensor platform for remote refractive index sensing.

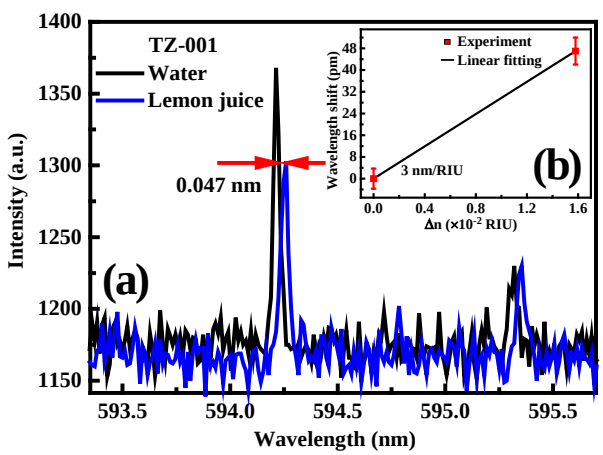

Fig. 8. (a) Lasing spectra of the R6G-doped TZ-001 polymer micro-ring laser in water and lemon juice. (b) The inset shows the lasing peak shifts as a linear function of refractive index change.

4. Conclusions

In this paper, we successfully demonstrated the versatility and robustness of the dye-doped polymer laser-based remote refractive index sensing platform. The simplicity of polymer deposition process and chemical resistance of patterned fused-silica substrate guaranteed the reproducibility and reusability of refractive index sensors. The comparisons of lasing spectral

Optics EXPRESS

characteristics show that the R6G-doped SU-8 micro-ring laser operating in the aqueous environment has narrower line widths and larger FSR than TZ-001. The lasing thresholds of both micro-scale lasers immersed in the water were measured to be 2.52 μJ/mm^2 and 15.5 μJ/mm^2, respectively. The characterization of lasing spectra of both micro-ring lasers within the different time intervals verified their reliable photostability as refractive index sensors. By repeatedly changing between the water and lemon juice, the sensitivity and DL of R6G-doped SU-8 polymer laser-based refractive index sensor were estimated to be 75 nm/RIU and 4×10^{-4} RIU, respectively. Similarly, the sensitivity and DL of R6G-doped TZ-001 polymer laser-based refractive index sensor were estimated to be 3 nm/RIU and 1×10^{-2} RIU, respectively. Therefore, the simple realization of polymer WGM micro-ring lasers-based refractive index sensors demonstrate their flexibility and potential use in remote environmental, chemical, bio-chemical, and biological sensing. The choice of the free-space optics measurement setup demonstrated in our work has paved a way towards realizing true remote sensing technology [39].

Funding

National Science Foundation (NSF) (DBI-1451127, CMMI-1727918); National Natural Science Foundation of China (NSFC) (61435006, 61525502, 61705046); Research fund for the Science and Technology Planning Project of Guangdong Province (2017B010123005); Postdoctoral Scientific Foundation of China (2017M6121608).

Acknowledgments

The authors gratefully thank Q. Y. Cui from the Michigan of University for experimental assistance. We would also like to acknowledge the technical support from Lurie Nanofabrication Facility (LNF) at the University of Michigan.